Research Article

Cancer Immunology Research

Customized Viral Immunotherapy for HPV-Associated Cancer

Matthew J. Atherton[1], Kyle B. Stephenson[2], Jonathan Pol[1], Fuan Wang[1], Charles Lefebvre[3], David F. Stojdl[2,3], Jake K. Nikota[2], Anna Dvorkin-Gheva[1], Andrew Nguyen[1], Lan Chen[1], Stephanie Johnson-Obaseki[4], Patrick J. Villeneuve[5], Jean-Simon Diallo[6], Jim Dimitroulakos[6], Yonghong Wan[1], and Brian D. Lichty[1,2]

Abstract

The viral-transforming proteins E6 and E7 make human papillomavirus–positive (HPV^+) malignancies an attractive target for cancer immunotherapy. However, therapeutic vaccination exerts limited efficacy in the setting of advanced disease. We designed a strategy to induce substantial specific immune responses against multiple epitopes of E6 and E7 proteins based on an attenuated transgene from HPV serotypes 16 and 18 that is incorporated into MG1-Maraba virotherapy (MG1-E6E7). Mutations introduced to the transgene abrogate the ability of E6 and E7 to perturb p53 and retinoblastoma, respectively, while maintaining the ability to invoke tumor-specific, multifunctional $CD8^+$ T-cell responses. Boosting with MG1-E6E7 significantly increased the magnitude of T-cell responses compared with mice treated with a priming vaccine alone (greater than 50×10^6 E7-specific $CD8^+$ T cells per mouse was observed, representing a 39-fold mean increase in boosted animals). MG1-E6E7 vaccination in the HPV^+ murine model TC1 clears large tumors in a $CD8^+$-dependent manner and results in durable immunologic memory. MG1-Maraba can acutely alter the tumor microenvironment *in vivo* and exploit molecular hallmarks of HPV^+ cancer, as demonstrated by marked infection of HPV^+ patient tumor biopsies and is, therefore, ideally suited as an oncolytic treatment against clinical HPV^+ cancer. This approach has the potential to be directly translatable to human clinical oncology to tackle a variety of HPV-associated neoplasms that cause significant morbidity and mortality globally. *Cancer Immunol Res; 5(10); 847–59. ©2017 AACR.*

Introduction

Human papillomavirus (HPV) infection plays a significant role in the pathogenesis of multiple epithelial malignancies, including virtually all cases of cervical carcinoma as well as many head and neck cancers (1). The vast majority of HPV cancers are triggered by two high-risk serotypes, HPV16 and 18 (2). In 2012, it was estimated that there were over half a million new cases of cervical cancer globally alongside a startling increase in the incidence of oropharyngeal tumors secondary to HPV infection in the developed world (3, 4). These malignancies remain a highly significant cause of morbidity and mortality, thereby mandating the need for new and efficacious treatments.

Foreign viral-transforming proteins are essential for the neoplastic phenotype of HPV^+ cancers. E6 and E7 early genes encode for proteins that impair cell-cycle control and inhibit apoptosis primarily via interaction with p53 and retinoblastoma (pRb), respectively (5). In human cells, E6 and E7 also render HPV^+ cells hyporesponsive to type I interferons (IFN; ref. 6). Although foreign viral antigens seemingly make HPV-associated cancer an ideal target for therapeutic vaccination, current data suggest that tumor-induced immunosuppression associated with advanced disease prevents vaccine monotherapy from being effective (7–10). Although some vaccines are efficacious against early-stage HPV-associated cancer, they are of minimal benefit in advanced disease.

Oncolytic viruses (OV) are a promising new class of cancer therapeutics. Cellular dysregulation, including type I IFN signaling defects, occurs during carcinogenesis and facilitates selective viral oncolysis, facilitating direct neoplastic cytotoxicity and induction of antitumor immunity (11, 12). Following an extensive screening process, the attenuated, IFN-sensitive MG1 strain of Maraba virus was identified as a highly selective and potent rhabdoviral OV capable of lethally infecting various human and murine tumor cells both *in vitro* and *in vivo* (13). MG1-Maraba can also act as a powerful anticancer vaccine platform. Mice primed with a replication-deficient adenovirus expressing dopachrome tautomerase (DCT) display potent anti-DCT immune responses when subsequently boosted with MG1-DCT, which enhanced survival in a melanoma model (14). Given this platform's remarkable potency as a vaccine, we hypothesized that the application of a custom-designed, tetravalent transgene would be efficacious against a model of

[1]McMaster Immunology Research Centre, Department of Pathology and Molecular Medicine, McMaster University, Hamilton, Canada. [2]Turnstone Biologics, Ottawa, Canada. [3]Stojdl Lab, CHEO Research Institute, Children's Hospital of Eastern Ontario, Ottawa, Canada. [4]Department of Otolaryngology-Head and Neck Surgery, The Ottawa Hospital, Ottawa, Canada. [5]Department of Surgery, The Ottawa Hospital, Ottawa, Canada. [6]Centre for Cancer Therapeutics, The Ottawa Hospital Research Institute, and Faculty of Medicine and the Department of Biochemistry at the University of Ottawa, Ottawa, Canada.

Note: Supplementary data for this article are available at Cancer Immunology Research Online (http://cancerimmunolres.aacrjournals.org/).

Corresponding Author: Brian D. Lichty, McMaster University 1200 Main Street West MDCL 5023, Hamilton, Ontario L8N 3Z5, Canada. Phone: 905-521-2100; Fax: 905-525-6750; E-mail: lichtyb@mcmaster.ca

doi: 10.1158/2326-6066.CIR-17-0102

advanced HPV$^+$ cancer, and therefore we constructed MG1-E6E7. A further rationale for adopting MG1 therapy against HPV$^+$ tumors comes from the observation that xenografted models of HPV$^+$ cancer cell lines are susceptible to rhabdoviral oncolysis (15). We demonstrate induction of specific CD8$^+$ T-cell responses resulting in complete tumor regression in 75% of immune-competent mice bearing advanced tumors and selectively enhanced MG1 replication in primary HPV$^+$ human tumor biopsies. Thus, HPV-associated tumors are bespoke targets for precision-designed virotherapy with MG1-E6E7.

Materials and Methods

Mice

Female C57BL/6 mice age 6 to 8 weeks were purchased from Charles River Laboratories and housed in specific pathogen-free conditions. Studies were approved by McMaster University's Animal Research Ethics Board and complied with Canadian Council on Animal Care guidelines.

Recombinant viruses

Codon-optimized transgenes encoding the attenuated E6E7 and WT E6E7 sequences (Fig. 1A) were manufactured (GensScript). Ad-BHG (no transgene) and Ad-E6E7 (encodes the attenuated E6E7 construct) are human serotype 5 replicate-deficient (E1/E3 deleted) adenoviruses. The previously described double mutant MG1-Maraba virus (13) was manufactured in the Stojdl Lab (University of Ottawa), the GFP or E6E7 transgenes were inserted between the G and L viral genes of MG1-Maraba virus to produce MG1-GFP and MG1-E6E7, respectively.

Cell culture

TC1 cells were cultured in RPMI containing 10% fetal bovine serum (FBS), HEPES (10 mmol/L), L-glutamine (2 mmol/L), and G418 (400 μg/mL; Gold Biotechnology). HPV16 E6 and E7 expression was confirmed by RT-PCR (Supplementary Fig. S1), and cells were passaged for 1 week maximum prior to engraftment. Vero 76 and A549 cells were cultured in αMEM containing 10% FBS and L-glutamine (2 mmol/L). L929 cells were cultured in αMEM containing 8% FBS and L-glutamine (2 mmol/L). SaOS2 and HEK293T cells were cultured in DMEM containing 10% FBS and L-glutamine (2 mmol/L). All lines tested negative for *Mycoplasma* using TLR2 and PCR assays between 2011 and 2017. TC1 cells were a gift from Dr. Webb (B.C. Cancer Agency) in 2013, Vero 76 were purchased from ATCC in 2012. L929 and HEK293T cells were a gift from Dr. Bell (University of Ottawa) in 2007 and 2008, respectively. A549 were a gift from Dr. Bramson (McMaster University) in 2007, and SaOS2 were a gift from Dr. Mossman (McMaster University) in 2010. Vero 76, L929, A549, SaOS2, and HEK293T used for transfections and viral propagation had conformant morphology, culture, infection, and transfection characteristics. Vero 76 had epithelial morphologic features and grew in adherent monolayers exhibiting viral plaques and cellular cytopathia following rhabdoviral infection. L929 had fibroblastic morphologic features, grew in adherent monolayers, and expressed murine-specific β-actin by RT-PCR (Supplementary Fig. S1). A549 had epithelial morphologic features, grew in adherent monolayers, expressed wild-type p53, and had an inducible antiviral state following transfection. SaOS2 and HEK293T had epithelial morphologic features, grew in adherent monolayers, and were both readily transfectable.

Western blotting and antibodies

Equivalent amounts (20–30 μg per lane) of protein lysates were loaded onto polyacrylamide gels, separated by SDS-PAGE, and transferred to nitrocellulose membranes (Santa Cruz Biotechnology). Membranes were blocked with 5% fat-free milk in PBS or Odyssey Blocking Buffer (LI COR Biosciences) for 40 minutes and probed with antibodies against p53 (clone DO1; Santa Cruz, Biotechnology), HA (clone F7; Santa Cruz Biotechnology), E7 (clone 8E2; Abcam), β-actin (clone 13E5; Cell Signaling Technology), and GFP (clone D5.1; Cell Signaling Technology). Membranes were then probed with secondary IRDye (LI COR Biosciences) antibodies and scanned. Fluorescence was quantified using the LI COR Odyssey system (LI COR Biosciences).

Transient transfections

A549 cells were transfected in 6-well plates when cells were ∼80% confluent with 2 μg of WT E6E7, attenuated E6E7, or GFP in a pShuttle-CMV vector (Agilent) using Lipofectamine 2000 (ThermoFisher Scientific). SaOS2 cells were cotransfected in 6-well plates when cells were ∼80% confluent with HA-tagged retinoblastoma in pcDNA 3 (Gift from Dr. Mymryk), GFP, and either WT E6E7, attenuated E6E7, or empty pShuttle-CMV. Cells were lysed in 100 μL of radioimmunoprecipitation assay (RIPA) buffer (10 mmol/L phosphate pH 7.4, 137 mmol/L NaCl, 1% NP-40, 0.5% sodium deoxycholate, and 0.1% SDS) supplemented with complete Mini protease inhibitor tablets (Roche) 24 to 48 hours after transfection.

Immunoprecipitation

Approximately 90% confluent HEK293T cells in 60-mm dishes were transfected with HA-tagged Rb (WT) or Flag-tagged E6E7 (WT and mutants) in pcDNA3.1 using XtremeGENE HP DNA transfection reagent (Roche). For Western blots (WB), treated cells were lysed in RIPA supplemented with protease inhibitor cocktail (Roche) and phosphatase inhibitor cocktail II + III (Sigma-Aldridge), 30 μg of lysate was loaded per lane, and WBs were run and imaged as above. For immunoprecipitations (IP), cells treated as detailed above were lysed in IP buffer (20 mmol/L Tris–HCl pH 7.4, 137 mmol/L NaCl, 1 mmol/L EDTA, 1% NP-40, 10% glycerol and protease/phosphatase inhibitor cocktail (ThermoFisher Scientific). Cellular lysates (400 μL) were incubated with rabbit anti-HA conjugated to Sepharose beads (Clone C29F4, Cell Signaling Technology) at 4°C for 3 hours. Immunoprecipitates were washed thoroughly and boiled in 96 μL of SDS sample buffer. Boiled immunoprecipitates (15 μL) were loaded onto polyacrylamide gels, and WB was performed using anti-Flag (Clone 9A3, Cell Signaling Technology) or anti-HA (Clone 6E2, Cell Signaling Technology).

Tumor challenge

Mice were engrafted with 1×10^6 TC1 cells subcutaneously under gaseous general anesthesia. Tumor volumes were measured using digital calipers (iGAGING), and mice were weighed every 2 to 3 days.

Tumor volume was calculated using the following formula:

$$\text{Volume} = 4/3\pi\left(0.5 \text{ length} \times [0.5 \text{ width}]^2\right)$$

Endpoints were 1,500 mm^3 tumor volume, 20% body-weight loss, or moribund secondary to weight loss.

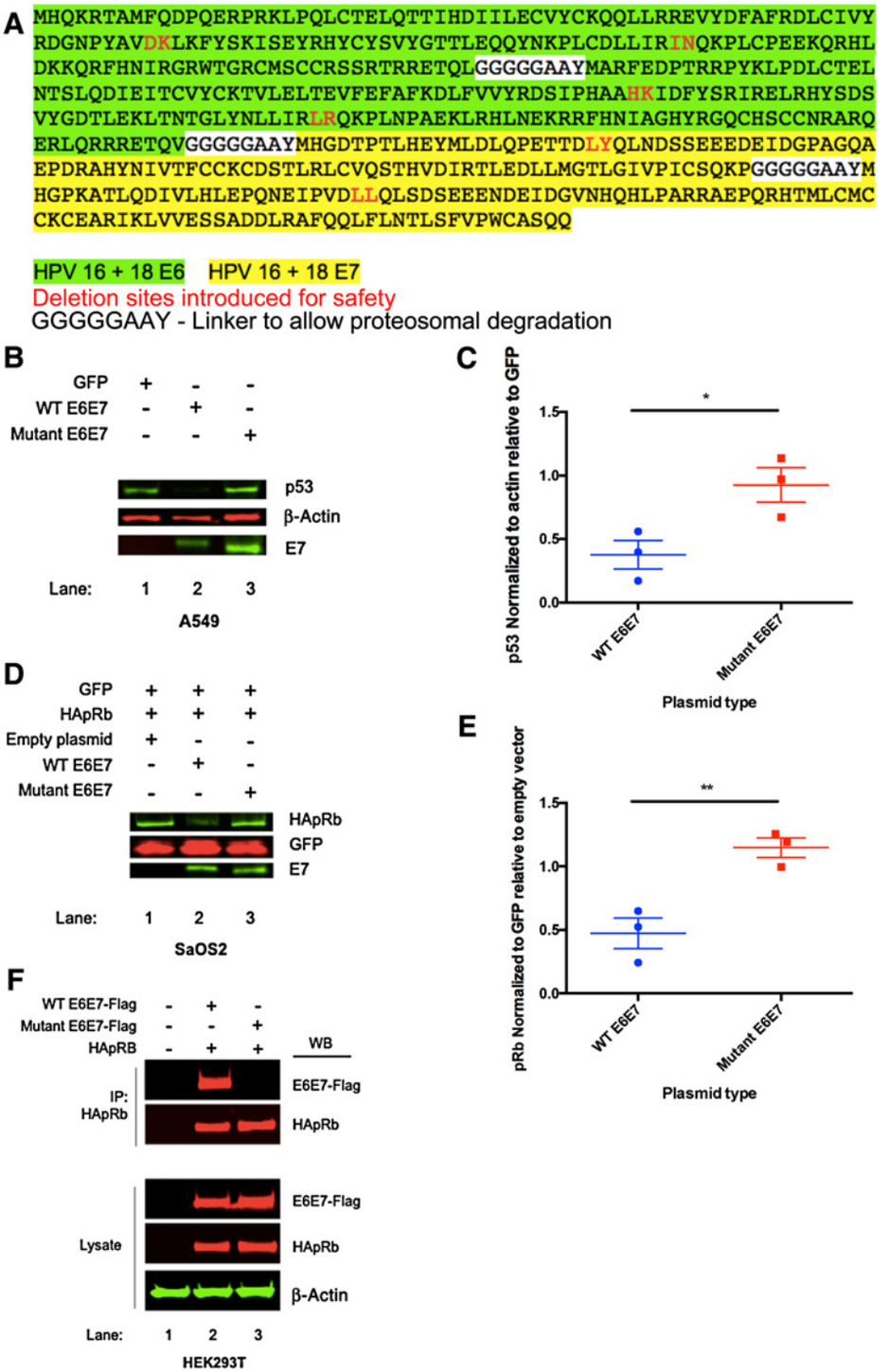

Figure 1.

Tetravalent transgene design, sequence, and effects on p53 and pRb. **A,** Peptide sequence of the transgene cloned into an adenoviral priming vector and MG1-E6E7. Sequences are highlighted as follows: E6 in green, E7 in yellow, and linkers in white. Red characters indicate mutation sites introduced for safety. **B,** A549 cells were transfected with plasmids encoding the therapeutic and WT E6E7 transgenes, and lysates were probed for p53. **C,** Densitometry on Western blots. Three independent transfections performed. Mean and SEM displayed; comparison performed using an unpaired (Student's) two-tailed *t* test: *, $P \leq 0.05$. **D,** Retinoblastoma null SaOS2 cells were cotransfected with plasmids encoding therapeutic or WT E6E7 alongside HA-tagged retinoblastoma and GFP. Lysates were probed for retinoblastoma. **E,** Densitometry on Western blots. Three independent transfections performed. Mean and SEM displayed; comparison performed using an unpaired (Student's) two-tailed *t* test, **, $P \leq 0.01$. **F,** Immunoprecipitation of flag-tagged therapeutic and WT E6E7 sequences were performed using HA-tagged retinoblastoma in HEK293T cells.

Vaccination of mice

Adenovirus (2×10^8) PFU in 100 μL of 0.9% NaCl (Hospira) was administered (50 μL per semimembranosus muscle) under general anesthesia. For prime boost studies, a single dose 1×10^9 PFU MG1 was administered intravenously (i.v.) in 200 μL 0.9% NaCl 9 days after adenovirus injection. For direct oncolysis, mice received 2 i.v. doses of 1×10^9 PFU MG1-GFP 48 hours apart. Mice received initial viral treatments with a mean tumor volume of approximately 300 mm^3.

Peptides

Immunodominant peptides from HPV serotype 16 were synthesized by Biomer Technologies. Sequences were as

follows: H-2K^b E6 peptide-EVYDFAFRDL and H-2D^b E7 peptide-RAHYNIVTF.

Intracellular cytokine staining and antibodies

Blood was acquired retro-orbitally 8 days after adenovirus injection, and blood as well as spleens were harvested 5 days after the MG1 dose. PBMCs ($\sim 1.5 \times 10^5$) and splenocytes ($\sim 7.5 \times 10^5$) were incubated in 96-well plates at 37°C/5% CO_2/95% humidity for 5 hours with peptide (2 μg/mL) and anti-CD107a (clone 1D4B; BD) in RPMI containing 10% FBS and L-glutamine (2 mmol/L). Brefeldin A (1 μg/mL; GolgiPlug, BD) was added for the last 4 hours. Cells were then incubated at 4°C for 10 minutes with anti-CD16/CD32 (clone 2.4G2; Mouse BD Fc Block, BD). T-cell surface staining was performed using anti-CD8a (clone 53-6.7; eBiosciences, Inc.) and anti-CD4 (clone RM4-5; eBiosciences, Inc.). Cells were subsequently fixed and permeabilized (Cytofix/Cytoperm, BD), and intracellular cytokine staining (ICS) was performed using anti-IFNγ (clone XMG1.2; BD), anti-TNFα (clone MP6-XT22; BD), and anti-IL2 (clone JES6-5H4; BD). Data were acquired using an LSR FORTESSA cytometer (BD) and analyzed with FlowJo for Mac (TreeStar).

T-cell counts

Fluorescent beads (50 μL) at a known concentration (123 count eBeads, eBiosciences, Inc.) were added to 50 μL of whole blood that had been stained with antibodies against CD8a (clone 53-6.7; eBiosciences, Inc.) and CD4 (clone RM4-5; eBiosciences, Inc.) and fixed as well as lysed (1-step Fix/Lyse solution, eBiosciences, Inc.). The cells and beads were resuspended in FACS [0.5% bovine serum albumin (Equitech-Bio, Inc.) in PBS] after 2 wash steps. Data were acquired and analyzed as above. Absolute CD8$^+$ and CD4$^+$ cells per μL blood were calculated using the following formula:

$$\text{Absolute count(cells/μl)} = (\text{cell count/eBead count}) * \text{eBead concentration}$$

Total blood volume in microliters was calculated by multiplying each mouse's body weight in grams by 70, thus allowing a total circulating count of T cells. For enumeration of splenocytes, the entire spleen was processed and resuspended in a known volume of complete RPMI. Splenocytes (50 μL) in RPMI suspension were then analyzed with counting beads as for peripheral blood. Total numbers of antigen-specific T cells were calculated using the product of absolute CD8$^+$ counts and frequencies of specific T cells as determined by ICS.

T-cell memory phenotype and antibodies

PBMCs ($\sim 1.5 \times 10^5$) and splenocytes ($\sim 7.5 \times 10^5$) were incubated with anti-CD16/CD32 (clone 2.4G2, Mouse BD Fc Block, BD) at 4°C for 10 minutes. Cells were then stained with anti-CD8a, anti-CD4, anti-CD62L (clone MEL-14; BD), anti-CD127 (clone SB/199; BD), and HPV H-2D^b E7 tetramer RAHYNIVTF (Baylor College of Medicine).

Depletion antibodies

T cells were selectively depleted by injecting 200 μg of anti-CD8a (clone 2.43) or anti-CD4 (clone GK1.5) intraperitoneally. Mice received 2 injections of depleting antibodies 48 hours apart, and depletion was assessed flow cytometrically from peripheral blood samples taken 7 days after the first dose of antibody for early depletions and 3 days after the first dose of antibody for late depletions.

In vitro infections

Six-well plates containing confluent TC1 cells were infected with MG1-GFP at decreasing multiplicity of infection (MOI; from 10 to 0.001, including an uninfected control) in 200 μL of culture medium for 45 minutes. Following infection, fresh medium was added, and 48 hours after infection, cells were methanol-fixed and stained with 0.1% crystal violet (Sigma-Aldridge) in 20% ethanol for viability.

Intratumoral viral titers

Established TC1 tumors were harvested and snap frozen 12 and 24 hours after mice received i.v. injections of 1×10^9 PFU MG1-GFP. Tumors were stored at −80°C prior to homogenization and subsequent plaque assay on Vero 76 cells.

nanoString hybridization

Tumors were harvested 24 hours after i.v. injection of 1×10^9 PFU MG1-E6E7 alongside tumors from untreated mice. Tumors were stored in RNAlater (Sigma-Aldridge) prior to RNA extraction using TRIzol (Thermo Fisher Scientific). All samples had RNA integrity numbers (RIN) of at least 8.9 as determined by a 2100 Bioanalyzer (Agilent) using RNA Nano Chips (Agilent). The nCounter Mouse Immunology panel was used to examine differential expression of mRNAs. Each tumor contributed 1 sample. Total RNA (50 ng) in 5 μL was hybridized at 65°C for 21 hours, and data were acquired using nCounter Max Analysis System. Profiled data were preprocessed following the manufacturer's recommendations. Specifically, background was subtracted by using geometric mean of the negative controls, and normalization was performed using positive controls and housekeeping genes using nSolver software, and obtained values were Log_2 transformed. To visualize sample distribution, whole profiles were used for the hierarchical clustering (Euclidean distance, complete linkage) and principal component analysis (PCA). Profiles were analyzed for differential expression by using *limma* package in R (16).

G-deleted vesicular stomatitis virus (VSV) assay

A549 human lung adenocarcinoma cells were seeded in a 6-well plate and cotransfected at 90% confluence using Lipofectamine 2000 (ThermoFisher Scientific), a plasmid of interest, and a plasmid encoding VSV glycoprotein PSG5-G. Cells were subsequently infected with a G-deleted VSV expressing GFP, and supernatants were harvested. Supernatants containing rescued viral progeny were collected, serially diluted, and used to infect confluent Vero 76 cells in a 96-well plate. Fluorescence was visualized using a Typhoon Trio Variable Mode Imager (GE Healthcare). Fluorescence was quantified using ImageQuant TL software (GE Healthcare).

Ex vivo tumor analysis

Tumor tissues from head and neck squamous cell carcinoma (HNSCC) patients undergoing routine surgical procedures were obtained and analyzed (approved by the Ottawa Hospital Research Ethics Board; Protocol# 20120559-01H). HPV$^+$ patients were determined by positive immunohistochemistry for p16, a routinely used surrogate marker of HPV (17). Areas containing tumor were identified by gross tissue examinations.

Approximately 2 mm cores were obtained using a sterile biopsy punch and further dissected to approximately 2 × 1 mm slices. Slices were randomized, and two slices were placed into each well of 24-well plate and cultured in DMEM supplemented with 10% FBS and antibiotic/antimycotic solution (100 units/mL; Sigma-Aldridge). After 48 hours of MG1-GFP infection at 1×10^7 or 5×10^7 PFU (or both when adequate tissue available), slices were rinsed twice with PBS and processed for viral titration as previously described (18). Bright field and fluorescent images of tumors were captured with EVOS FL Cell Imaging System (ThermoFisher Scientific) at 4× magnification.

Statistical analyses

Data were displayed and analyzed using GraphPad Prism (GraphPad Software). Two-tailed unpaired (Student) *t* tests or Mann–Whitney tests were used when comparing two groups, and ANOVA tests were used to compare greater than two groups. Tumor endpoint survival was plotted using Kaplan–Meier curves, and median survival was compared using the log-rank tests. Statistical significance was defined as $P \leq 0.05$ (*, $P \leq 0.05$; **, $P \leq 0.01$; ***, $P \leq 0.001$; ****, $P \leq 0.0001$).

Results

The mutant E6E7 transgene does not degrade p53 or retinoblastoma *in vitro*

A quadrivalent mutated transgene was designed and cloned into the adenoviral and Maraba MG1 viruses based on the E6 and E7 proteins of HPV16 and 18. A linker sequence (GGGGGAAY) promoting proteasomal cleavage was inserted between each of the proteins to avoid generation of chimeric peptides. In both E6 domains, deletions were made to two of the four CXXC motifs, which mediate p53 degradation (Fig. 1A; ref. 19). A549 cells containing wild-type p53 were transfected with expression vectors encoding the WT E6E7 transgene, the mutated E6E7 transgene, or an irrelevant control plasmid (GFP), and p53 was then quantified by WB. p53 was degraded by WT E6E7, and degradation was completely inhibited in the mutant transgene compared with the GFP control (Fig. 1B and C). In both E7 domains of the mutated transgene, a deletion was applied to one of the carboxy-terminus CXXC motifs as well as deletions to the LXCXE sequences responsible for the dysfunction of pRb (20). SaOS2 cells were cotransfected with a plasmid encoding HA-tagged pRb (HApRb) alongside a GFP encoding plasmid, and one of the following three expression vectors: the WT E6E7 transgene, the mutant transgene, or a control plasmid. Following transfection, HApRb was quantified via WB. A significant decrease in the WT E6E7 transfected cell lysates was seen, and pRb degradation was abrogated in the mutant transgene compared with control transfections (Fig. 1D and E). Immunoprecipitation experiments in HEK293T cells revealed clear interaction between flag-tagged WT E6E7 and HApRb but no interaction between the flag-tagged mutant transgene and HApRb (Fig. 1F). Deletions introduced into the therapeutic transgene prevent destabilization of p53 and pRb tumor suppressors.

E6E7 vaccination induces specific T-cell responses against E6 and E7 epitopes

A vaccination strategy of an adenoviral prime encoding the mutant E6E7 (Ad-E6E7) followed by the MG1-Maraba virus boost (MG1-E6E7) was administered to mice, and immune responses were quantified using ICS. For comparison, sham prime (Ad-BHG) and boost (MG1-GFP) groups were analyzed. Peripheral blood mononuclear cells (PBMC) were restimulated with peptides for E6 and E7 of known C57BL/6 CD8$^+$ T-cell epitopes. Blood samples after Ad-E6E7 vaccination revealed specific responses against both epitopes, as indicated by the production of interferon-γ (IFNγ) from CD8$^+$ T cells. Responses against the E7 epitope were greater than those against the E6 epitope (Fig. 2A and B). Following MG1-E6E7, a significant increase in IFNγ$^+$ T-cell frequency was observed in mice that received the E6E7 prime boost. Again, the E7 epitope was dominant with a mean frequency of 68.87% of CD8$^+$ T cells producing IFNγ following restimulation. Small responses were seen after MG1-E6E7 was administered to naïve recipients after sham priming (mean of 0.21% of CD8$^+$ T cells producing IFNγ after E7 restimulation; Fig. 2C and D). To compare the true magnitude of the responses generated with Ad-E6E7 alone to the prime boost, a subset of mice was sacrificed following boosting, and ICS was performed after E7 peptide restimulation. The peripheral blood and splenic CD8$^+$ T cells were enumerated using fluorescent beads. The prime boost induced a significant expansion of total and E7-specific CD8$^+$ T-cell populations compared with Ad-E6E7 alone (Fig. 2E and F). Combined splenic and circulating pools of E7-specific, IFNγ-producing CD8$^+$ T cells totaled a mean absolute count of 4.1×10^7 following the prime boost ($n = 10$, range = $2.4–5.1 \times 10^7$). Epitope mapping performed on the spleens of vaccinated mice revealed multiple CD4$^+$ epitopes across all four arms of the transgene (Supplementary Fig. S2). Boosting with MG1-E6E7 was able to generate specific CD4$^+$ and CD8$^+$ T-cell responses against E6 and E7 epitopes with extensive expansion of effector cells.

E6E7 vaccination generates multifunctional T cells

To assess the quality of the immune response, multifunctional T-cell analysis was performed on prime boost vaccinated mice following E7 restimulation. Mice receiving Ad-E6E7 alone were used for comparison. In both groups, double- (IFNγ$^+$ TNFα$^+$) and triple-positive (IFNγ$^+$ TNFα$^+$ IL2$^+$) CD8$^+$ T cells were found in the circulatory and splenic pools (Fig. 3). When double- and triple-positive CD8$^+$ T cells were quantified, mice receiving the prime boost had significantly more of both populations. The degranulation marker, CD107a (LAMP1), was also included, and virtually all cytokine productive cells were CD107a positive (Supplementary Fig. S3). Vaccination with Ad-E6E7 generated small numbers of E7-specific CD8$^+$ T cells capable of producing multiple effector cytokines, and boosting with MG1-E6E7 significantly expanded these populations.

E6E7 vaccination results in complete tumor regression

Mice bearing subcutaneous TC1 tumors were primed once their tumors reached approximately 300 mm^3, and specific CD8$^+$ T-cell responses against both E6 and E7 were demonstrated using ICS. A significant expansion of E7-specific T cells was documented after boosting with MG1-E6E7 relative to all other groups. Spontaneous immunity was not detected in untreated animals (Fig. 4A and B). All untreated mice succumbed to tumor progression, whereas treatment with either a sham prime boost or prime sham boost delayed tumor progression. In the sham prime MG1-E6E7 group, mice only received a relevant treatment (single dose of MG1-E6E7) once tumors reached a mean volume of approximately 1,000 mm^3, and in a single mouse, this resulted in complete

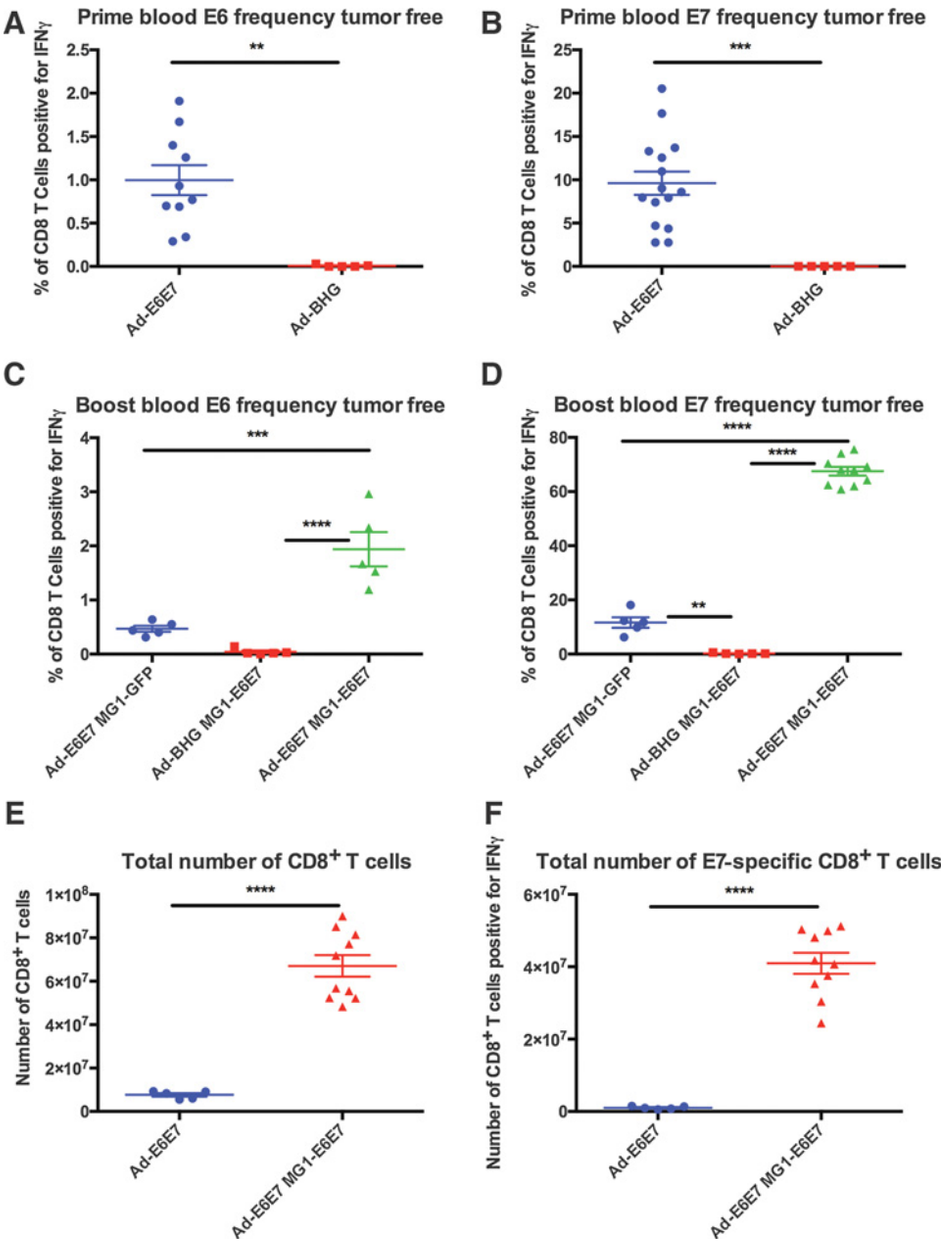

Figure 2.
Effects of E6E7 vaccination on immune responses. Tumor-free C57BL/6 mice were treated with various E6E7 vaccination regimens to assess the induction of specific immune responses against known E6 and E7 peptide epitopes. **A** and **B,** IFNγ production by $CD8^+$ T cells to (**A**) the E6 epitope ($n = 10$) and (**B**) the E7 epitope ($n = 15$) compared with sham-primed mice ($n = 5$). Mean and SEM displayed; comparisons performed using unpaired (Student) two-tailed *t* tests, **, $P \leq 0.01$; ***, $P \leq 0.001$. **C** and **D,** IFNγ production by $CD8^+$ T cells after boosting adenoviral-primed mice with MG1-E6E7 to (**C**) the E6 epitope ($n = 5$; **D**) the E7 epitope ($n = 10$) compared with sham-primed mice ($n = 5$) and sham-boosted mice ($n = 5$). Mean and SEM displayed; comparison performed using an ordinary one-way ANOVA; **, $P \leq 0.01$; ***, $P \leq 0.001$; ****, $P \leq 0.0001$. **E** and **F,** Enumeration of total splenic and circulating pools of (**E**) all $CD8^+$ (**F**) E7-specific $CD8^+$ T cells after MG1-E6E7 boost ($n = 10$) compared with animals receiving adenoviral priming alone ($n = 5$). Mean and SEM displayed; comparison performed using unpaired (Student) two-tailed *t* tests; ****, $P \leq 0.0001$.

sustained tumor regression (Supplementary Fig. S4). Treatment of mice bearing advanced TC1 tumors with Ad-E6E7 followed by MG1-E6E7 resulted in complete tumor responses in 75% of mice ($n = 12$; Fig. 4C), and $CD8^+$ T-cell depletion 2 days before boosting and subsequently forty days after boost resulted in loss of tumor control. No such effect was seen when $CD8^+$ cells were depleted at the later time point alone or when $CD4^+$ cells were depleted (Fig. 4D), suggesting the prime boost E6E7 vaccine generates specific immunity against E6 and E7 antigens, leading to complete regression in a $CD8^+$ T cell–dependent manner.

Long-lived antigen-specific immunity is observed after complete regression

T cell–memory phenotype was assessed in surviving mice with complete tumor clearance. Circulatory and splenic T cells were stained with an E7-specific tetramer, CD62L, and CD127 at 62 days and 117 days after MG1-E6E7 boosting (Fig. 5). Immune analysis revealed persistence of E7-specific $CD8^+$ T cells at both time points in the blood and spleen. The majority of the E7-specific cells were effector memory phenotype, and the relative proportions of central memory T cells significantly increased over time (5.1% in blood and 9.4% in spleen at 62 days post boost vs. 11.8% in blood and 18.8% in spleen at 117 days post boost; Supplementary Fig. S5). Oncolytic E6E7 vaccination generated long-lasting $CD8^+$ memory in mice cleared of advanced TC1 tumors.

MG1-Maraba is oncolytic and acutely alters the transcriptome of TC1 tumors

Oncolytic MG1-Maraba was cytotoxic to TC1 cells *in vitro* (Fig. 6A), and following tail-vein administration, viable MG1-GFP

was recovered from established TC1 flank tumors (Fig. 6B). Direct oncolysis alone did not result in tumor clearance, but treatment with MG1-GFP exerted antineoplastic activity, with 50% of mice exhibiting clear reduction in tumor volume (Fig. 6C). Within 24 hours of administration of MG1-E6E7, transcripts of various immune-related genes were altered within the tumor. NanoString analysis of mRNA isolated from 5 tumors treated with a single dose of MG1-E6E7 alone was performed and revealed increased expression of 17 genes primarily encompassing genes related to antigen presentation and innate viral sensing compared with 3 untreated tumors (Fig. 6D). PCA revealed distinct clustering of treated tumors compared with untreated controls (Supplementary Fig. S6). *IL1b* was the only gene in the panel expressed at a lower level than controls following MG1-E6E7. These data show that MG1-Maraba's oncolytic activity broadens its therapeutic profile beyond that of a conventional viral vaccine vector.

E6 and E7 diminish type I IFN responsiveness in human tumor cells

Human tumor cells transfected with WT E6 and E7 had decreased protection against rhabdoviral infection (Fig. 7A and B). Innate responses inhibit rhabdoviral infection of A549 cells. However, proteins known to diminish type I IFN responsiveness, such as measles V, enhance infection (21). In the absence of the G-plasmid (PSG5-G), G-deleted VSV-GFP is unable to produce viral progeny. Only cells that were successfully transfected with PSG5-G aided by inhibition of the anti-viral state by the transfected plasmid of interest are able to produce fluorescent viral progeny (21). Transfection of A549 cells with WT E6E7 significantly increased susceptibility to infection relative to a control plasmid, and the magnitude of increase was comparable with measles V (Fig. 7A and B). HPV-associated head and neck cancer patient biopsies were infected *ex vivo* with MG1-GFP. Following infection, fluorescence was confirmed microscopically (Supplementary Fig. S7), and viral titrations from biopsies were performed. All HPV$^+$ tumors were permissive to MG1 infection, with the HPV$^+$ tumors displaying significantly enhanced viral replication (Fig. 7C), illustrating that expression of E6 and E7 renders human tumor cells more permissive to MG1 replication.

Discussion

Due to the intrinsically foreign nature of HPV$^+$ tumors, many therapeutic vaccine approaches have been applied in the clinic but with limited success as single agents against advanced disease. Here, we describe a therapeutic approach in mice that induces complete and durable regression of the majority of advanced tumors with a mean volume of 300 mm^3 at the start of treatment. The heterologous prime boost regimen induces endogenous, specific CD8$^+$ T-cell responses with the potential to produce over fifty million E7-specific T cells per mouse. The ability of MG1 to acutely alter the transcriptional profile of the tumor microenvironment and preferentially replicate within HPV$^+$ patient biopsies justifies the rationale behind the design of this precision

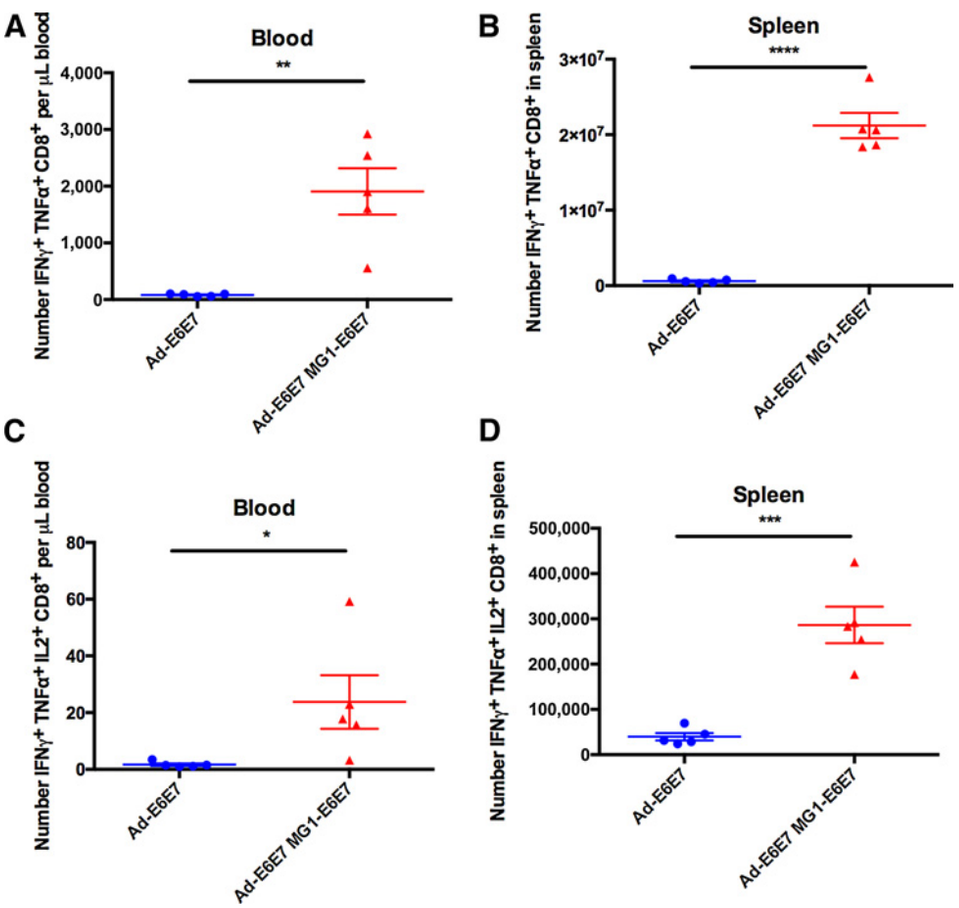

Figure 3.
Multifunctional E7-specific CD8$^+$ T-cell responses. Tumor-free C57BL/6 mice were treated with E6E7 priming and prime boost vaccines to assess the induction of E7-specific multifunctional CD8$^+$ T cells. Numbers of IFNγ^+ TNFα^+ CD8$^+$ T cells in (**A**) circulating and (**B**) splenic pools of boosted mice ($n = 5$) compared with mice treated only with the adenoviral priming vector ($n = 5$). Numbers of IFNγ^+ TNFα^+ IL2$^+$ CD8$^+$ T cells in (**C**) circulating and (**D**) splenic pools of boosted mice ($n = 5$) compared with mice treated only with the adenoviral priming vector ($n = 5$). Mean and SEM displayed; comparisons performed using unpaired (Student's) two-tailed *t* tests; *, $P \leq 0.05$; **, $P \leq 0.01$; ***, $P \leq 0.001$; ****, $P \leq 0.0001$.

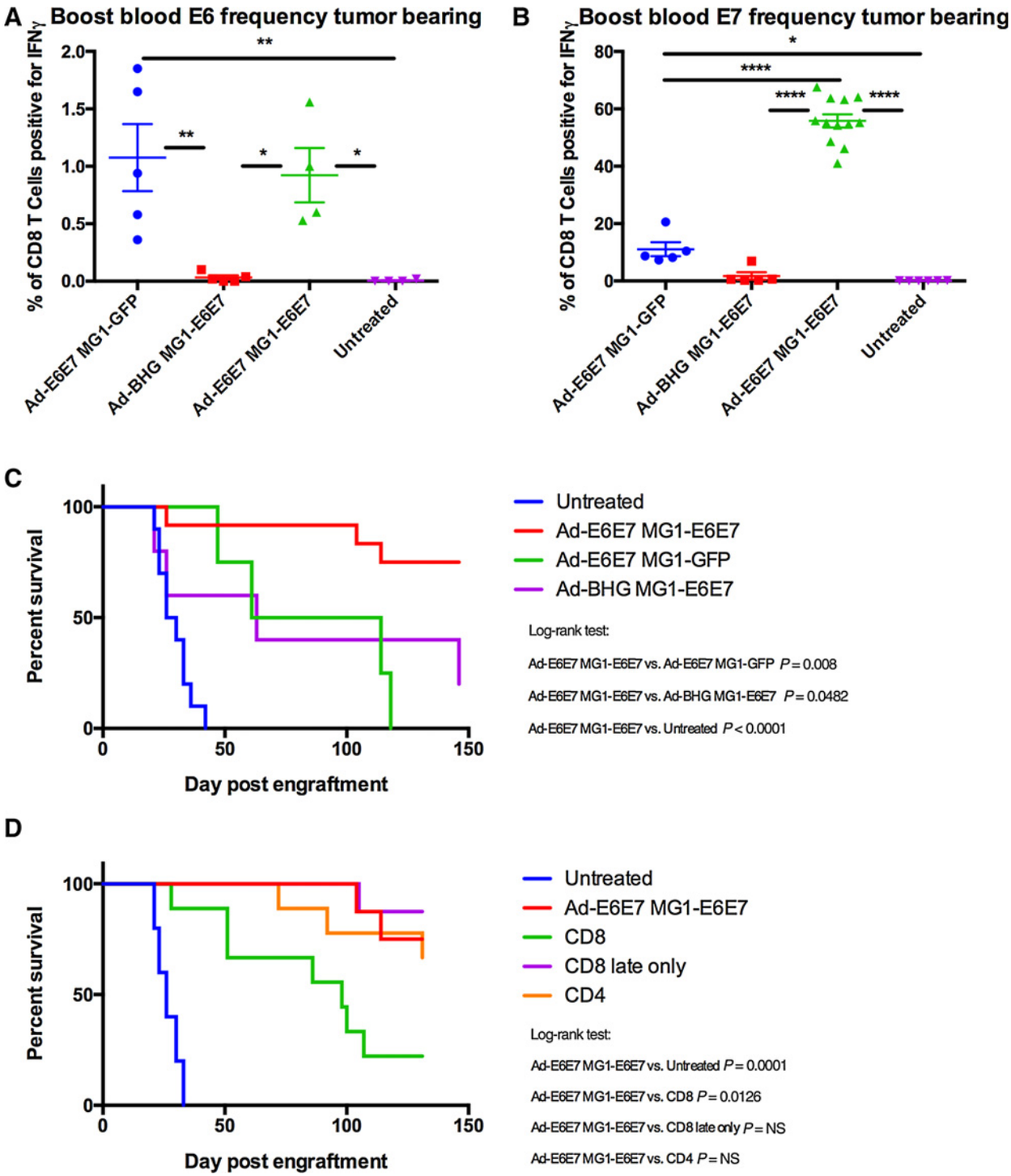

Figure 4.

CD8$^+$ T-cell responses and survival in E6E7-treated mice. C57BL/6 were engrafted 1×10^6 TC1 cells subcutaneously and treated with E6E7 vaccination therapy once tumors reached a mean volume of approximately 300 mm^3. **A,** Specific circulating CD8$^+$ T-cell responses to E6 peptide in prime boosted ($n = 4$), sham primed ($n = 5$), sham boosted ($n = 5$), and untreated ($n = 4$) tumor-bearing mice. **B,** Specific circulating CD8$^+$ T-cell responses to E7 peptide in prime boosted ($n = 12$), sham primed ($n = 5$), sham boosted ($n = 5$), and untreated ($n = 6$) tumor-bearing mice. Mean and SEM displayed; comparisons performed using ordinary one-way ANOVAs; *, $P \leq 0.05$; **, $P \leq 0.01$; ***, $P \leq 0.001$; ****, $P \leq 0.0001$. **C,** Long-term survival in mice treated with an adenoviral prime and MG1-E6E7 boosting ($n = 12$) in comparison with control mice ($n = 10$), sham boosted ($n = 4$), and sham primed mice ($n = 5$). Pooled data from 2 experiments. **D,** Early depletion of CD8$^+$ T cells in prime boosted mice ($n = 9$) compared with prime boosted nondepleted mice ($n = 8$), depletion of CD4$^+$ T cells ($n = 9$), late CD8$^+$ depletion ($n = 8$), and untreated mice ($n = 5$). Log-rank tests performed to compare survival curves.

therapy and shows potential for clinical application when combined with the vaccine's ability to generate such large numbers of T cells.

Mutations introduced to the therapeutic transgene neutralize the ability of E6 and E7 HPV proteins to interact with and destabilize p53 and pRb. Because Maraba is a rhabdovirus, it does not pose a risk of insertional mutagenesis due to DNA never being manufactured in the virus' life cycle, which is entirely extranuclear (13). The frequency of adenoviral integration into the host genome is low (22). However, if cells transduced with Ad-E6E7 were to undergo an integration event with the E6E7 transgene, the resultant protein could not interfere with the functions of p53 or pRb. By including the full-length sequences of E6 and E7 from HPV 16 and 18, the majority of patients with HPV-associated cancer would be eligible for treatment with this vaccine and have the potential to develop responses against multiple potential epitopes. The mutant E6E7 transgene is devoid of the potential to destabilize p53 and pRb while maintaining an ability to induce antigen-specific immunity.

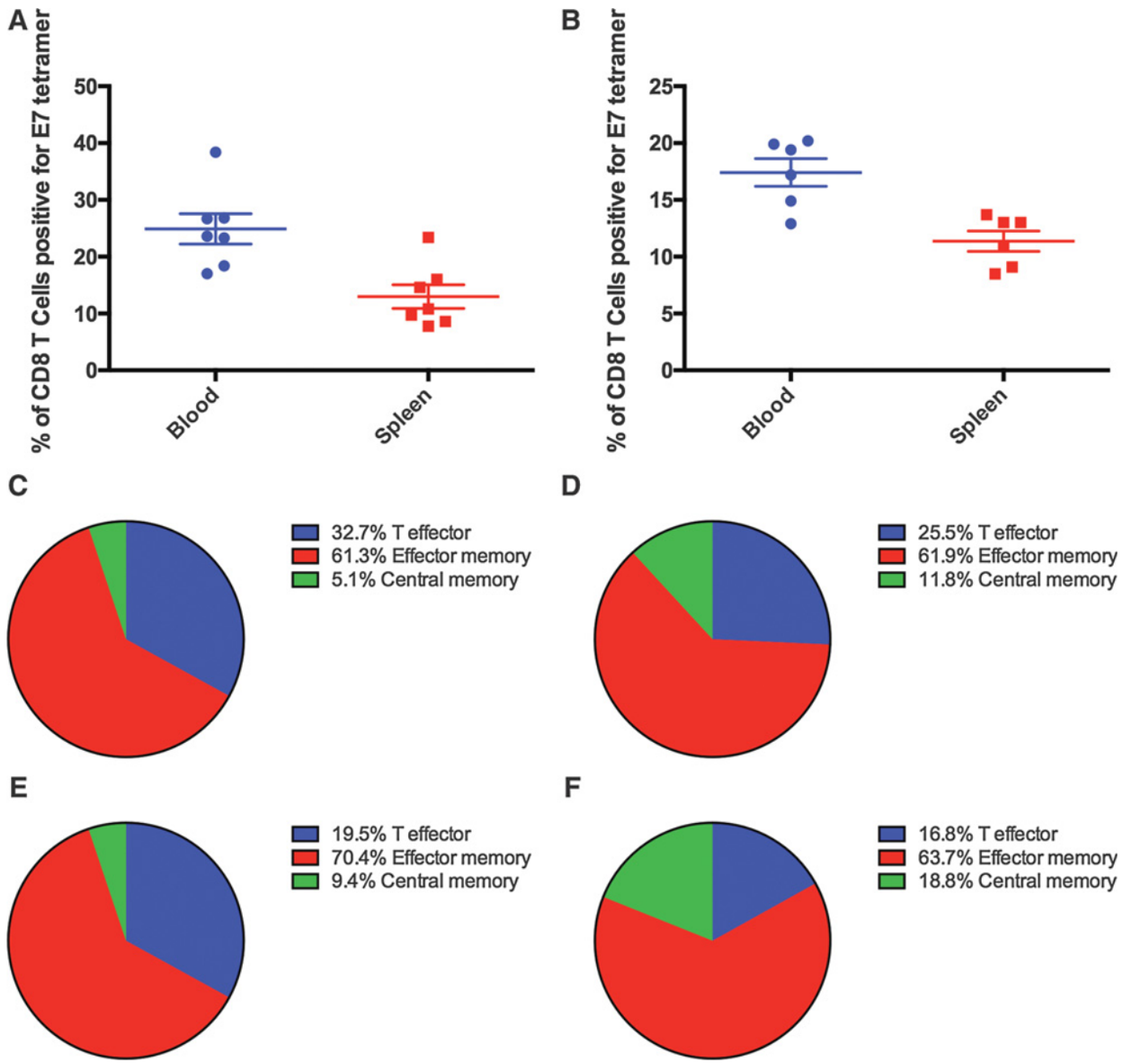

Figure 5.

Memory phenotype of E7-specific CD8$^+$ T cells. C57BL/6 mice that had complete regression of TC1 tumors following Maraba viral therapy were sacrificed to assess for persistence of specific E7 CD8$^+$ T cells and memory phenotype. Experiments were performed 62 days post MG1-E6E7 boosting ($n = 7$) and 117 days post MG1-E6E7 boosting ($n = 6$) with both circulating and splenic pools evaluated. Frequencies of total tetramer$^+$ CD8$^+$ T cells persisting at (**A**) day 62 and (**B**) 117 are shown. Relative proportions of the memory phenotypes of the T cells in (**C**) the blood at day 62, (**E**) the spleen at day 62, (**D**) the blood at day 117, and (**F**) the spleen at day 117 are displayed. Mean and SEM displayed for persistence experiments, and means displayed for memory phenotype experiments.

The dogma that the efficacy of an infectious disease vaccine is related to the ability of protective T cells being able to produce multiple cytokines is well established (23). Multiple different populations of T cells, defined by their pattern of cytokine production, are induced following E6E7 vaccination. Virtually all E7-specific, cytokine positive T cells are able to degranulate.

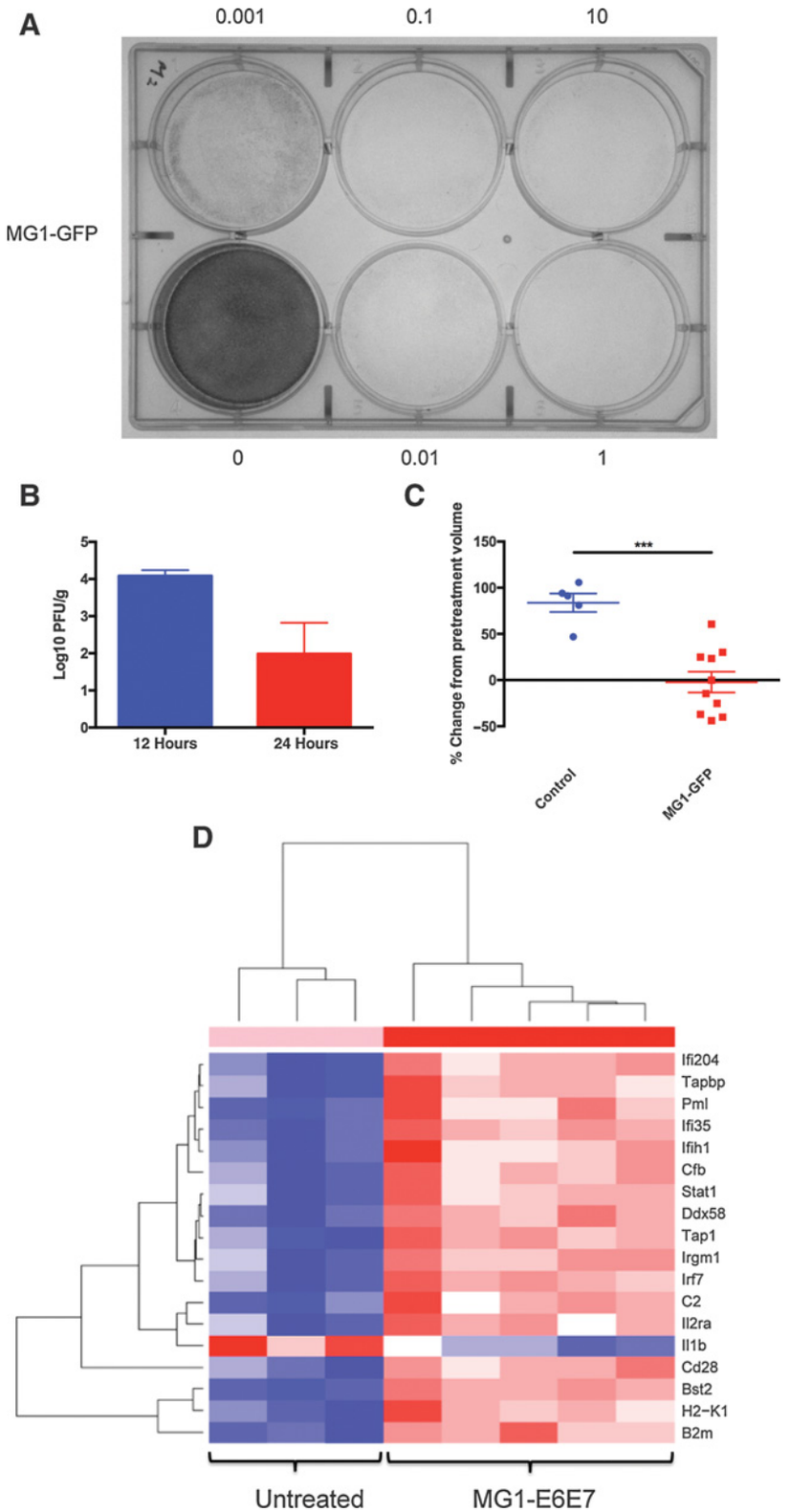

Figure 6.
MG1-maraba exerts oncolytic activity against established tumors. **A,** Monolayers of TC1 cells were cultured and infected with MG1-GFP at a variety of MOIs then subsequently stained with crystal violet. **B,** Established TC1 flank tumors were harvested from mice 12 ($n = 5$) and 24 ($n = 5$) hours after i.v. MG1-GFP and subjected to viral plaque assay. Mean and SEM displayed. **C,** Change in tumor volume 48 hours after systemic i.v. administration of oncolytic MG1-GFP. Mean and SEM displayed; comparison performed using an unpaired (Student) two-tailed t test; ***, $P \leq 0.001$. **D,** Genes differentially expressed within TC1 tumors 24 hours after treatment with systemic MG1-E6E7. mRNA was isolated from TC1 tumors of 5 mice treated with MG1-E6E7 and compared with 3 mice with untreated tumors. NanoString analysis using a murine immunology panel was undertaken, and genes with significantly altered expressions between groups (adjusted $P \leq 0.05$) are displayed using a heat map with increased and decreased expressions depicted by red and blue, respectively.

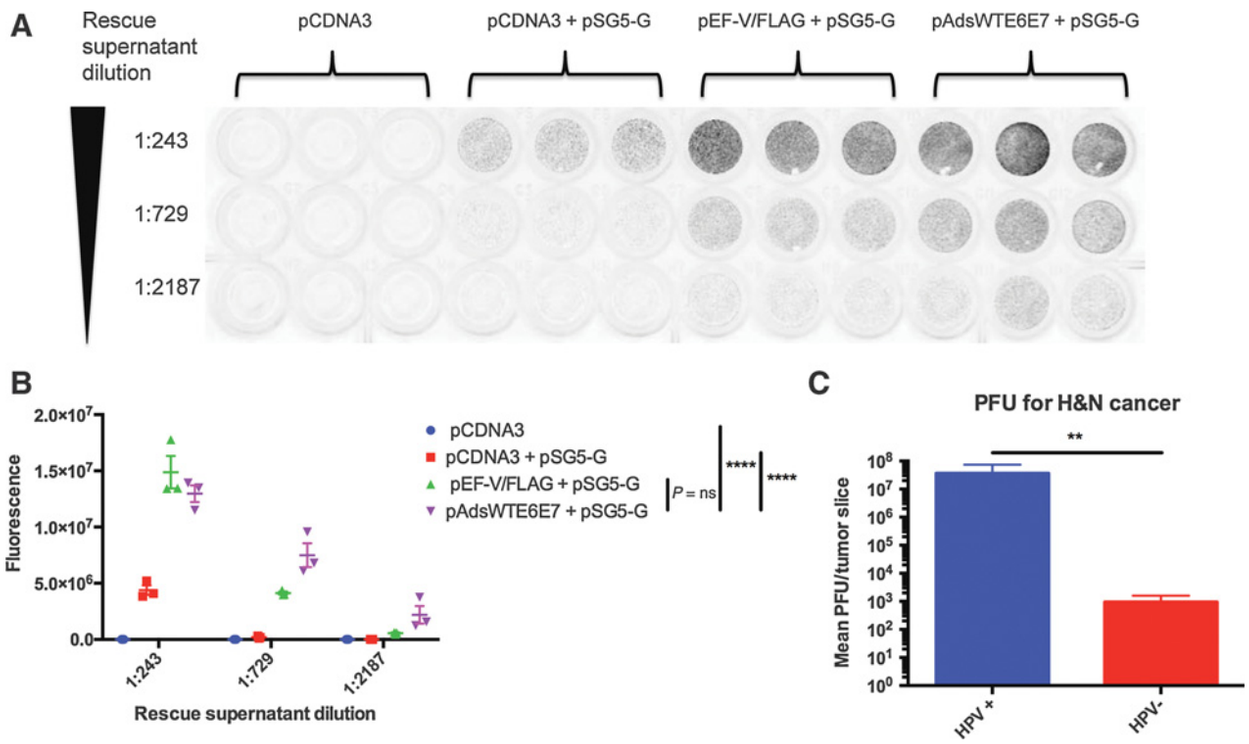

Figure 7.

G-deleted VSV assay and viral titrations. G-deleted VSV assay was performed on the human epithelial cancer line A549 following transfection with different plasmids. Infection was detected by fluorescence from a GFP transgene and is depicted by black signal. **B,** Fluorescence of wells was quantified using software and displayed graphically. Mean and SEM displayed; comparison performed using two-way ANOVA; ****, $P \leq 0.0001$. **C,** Biopsies of patients with HPV$^+$ ($n = 6$) and HPV$^-$ ($n = 11$) head and neck cancer were infected with MG1-Maraba *ex vivo*, and viral titration assays were performed. Mean and SEM displayed; comparison performed using the Mann–Whitney test; **, $P \leq 0.01$.

Although Ad-E6E7 alone induces multifunctional T cells, the numbers of these cells are vastly increased when boosted by MG1-E6E7. The value of multifunctional T cells has also been recognized in the realm of therapeutic cancer vaccines (24). Boosting with MG1-E6E7 is able to generate significant numbers of antigen-specific IL2$^+$ CD8$^+$ T cells, which are a functionally important population for anticancer vaccine efficacy (25). The ability of this oncolytic platform to generate multifunctional T cells further highlights its profile as a therapeutic.

The oncolytic virotherapy described here generates specific antitumor cytotoxic T cells, and efficacy is lost with depletion of CD8$^+$ T cells. Intravenous administration of rhabdoviral vectors boost primary immune responses by optimally stimulating splenic central memory T cells in the absence of inhibitory effector T cells, which results in proliferation of antigen-specific T cells (26). In patients, the adoptive transfer of autologous tumor-infiltrating lymphocytes following *ex vivo* expansion has the ability to clear metastatic cervical carcinoma, and clinical outcome was correlated with specific measures of anti-E6 and E7 immunoreactivity (27). If a vaccine were to provoke sizeable specific immune responses, then one would also expect a favorable clinical outcome. A potent vaccine could be used to induce specific E6 and/or E7 responses in patients and enhance prognosis. Although the effect of the number of cells adoptively transferred into TC1-bearing mice has not been fully investigated, a positive correlation between the number of cells transferred and tumor responses in established murine melanomas outlines the requirement for large T-cell responses (28). Therapeutic HPV vaccination strategies incorporating recombinant Listeria and peptide-based technologies are being extensively evaluated clinically due to their ability to generate specific CD8$^+$ T-cell immunity (29). The responses generated by MG1-E6E7 are substantially greater in magnitude than those previously reported in the preclinical setting (30, 31). Other groups have been able to clear established TC1 tumors only when vaccines are administered with various other therapeutics leading them to speculate that vaccine-induced endogenous immunity is only likely to be effective when part of complex combination therapies (7, 32). Here, we demonstrated that a straightforward vaccination regimen of two separate injections was able to generate extremely robust endogenous immunity and could completely ablate large murine tumors. Vaccinated mice exhibited durable persistence of specific CD8$^+$ T cells with a relative expansion of central memory T cells over time. The lack of the latter is considered one potential cause for therapeutic cancer vaccination failure (24). The prime boost resulted in much more uniform regression of tumors, but we were also able to demonstrate a complete response following treatment with a sham prime MG1-E6E7. A single dose of systemic MG1-E6E7 permanently cleared a tumor comprising approximately 5% of the animal's body weight. We have shown in a model of advanced HPV$^+$ tumors that MG1-E6E7 vaccination can exert a therapeutic effect.

Within 24 hours of the systemic administration of the oncolytic virus MG1-E6E7, the intratumoral immune transcriptional profile was significantly altered. Genes associated with antigen presentation and processing including *Tapbp, Tap1, H2-K1*, and *B2m* were upregulated following treatment with MG1-E6E7. Loss of antigen presentation is recognized as a significant cause of failure for cancer immunotherapy, so therapeutic approaches to increase intratumoral MHCI expression are highly desirable (33). Alongside the induction of various genes associated with innate antiviral immune responses, increased expression of *Cd28* and *Il2ra* was also of interest. Both CD28 and IL2RA are receptor molecules with significant roles in the activity of T lymphocytes (34, 35). The exact mechanism by which MG1 is able to increase the expression of these genes and their respective roles within the tumor microenvironment remains to be determined. *Il1b* was the only gene to have reduced intratumoral expression following MG1-E6E7 treatment. IL1 is frequently observed within tumors and has been implicated in tumorigenesis and systemic inflammatory paraneoplastic syndromes (e.g., cachexia; ref. 36). Weight loss reminiscent of cachexia was observed in mice with progressing TC1 tumors, so investigating the potential role of IL1β in this process is indicated. MG1-Maraba was also directly cytotoxic to TC1 cells, and replicating MG1 virus was isolated from tumors distant to the injection site. An immunosuppressive microenvironment is considered a significant factor for the failure of conventional therapeutic cancer vaccines (37, 38). Infection of tumors by OVs results in a proinflammatory response in the microenvironment, thereby offering a potential solution to this roadblock (11). MG1-Maraba virus is a versatile agent that acutely exerts multiple effects supporting antineoplastic activity against large TC1 tumors.

Multiple papilloma viruses are tumorigenic in many mammals. However, infection is highly specific to the host species (39). When E6 and E7 integrate into the genomes of human cells, as with high-grade HPV malignancies, type I cellular IFN responses are inhibited (6). The data from the G-deleted VSV assay recapitulate this effect in a human epithelial cancer cell line. Primary HPV^+ head and neck tumor biopsies are highly permissive to MG1 infection compared with HPV^- samples, predicting the sensitivity of such tumors to therapeutic oncolysis. The ability of Maraba-MG1 to exploit the cellular hallmarks of HPV-associated malignancy renders such tumors excellent targets for this therapeutic modality.

Outcomes from therapeutic vaccination of patients suffering from advanced HPV^+ tumors have been disappointing. In established cancers, it has been proposed that modification of the tumor microenvironment by oncolytic viruses is one mechanism by which failure of vaccination monotherapy due to tumor-associated immunosuppression may be avoided (37). The data presented in this study reveal that this engineered and readily translatable immunotherapeutic for HPV can induce multifunctional, specific antitumor $CD8^+$ T cells capable of durably eradicating advanced TC1 tumors in mice. Combining this effect with the oncolytic activity of MG1-Maraba may provide a potential therapeutic application in patients who have advanced HPV^+ tumors.

Disclosure of Potential Conflicts of Interest

J. Pol, D.F. Stojdl, and B.D. Lichty are owners of the patent for a vaccine composition using an Adenoviral prime and Maraba virus boost to induce an immune response against antigens (Publication Number EP2958994 A1) D.F. Stojdl is a consultant/advisory board member for Turnstone Biologics. B.D. Lichty is Chief Technology Officer at and is a consultant/advisory board member for Turnstone Biologics. No potential conflicts of interest were disclosed by the other authors.

Authors' Contributions

Conception and design: M.J. Atherton, J. Pol, C. Lefebvre, Y. Wan, B.D. Lichty
Development of methodology: M.J. Atherton, K.B. Stephenson, J. Pol, C. Lefebvre, P.J. Villeneuve, J. Dimitroulakos
Acquisition of data (provided animals, acquired and managed patients, provided facilities, etc.): M.J. Atherton, K.B. Stephenson, J. Pol, F. Wang, J.K. Nikota, A. Nguyen, L. Chen, P.J. Villeneuve, J.-S. Diallo, J. Dimitroulakos
Analysis and interpretation of data (e.g., statistical analysis, biostatistics, computational analysis): M.J. Atherton, K.B. Stephenson, J. Pol, A. Dvorkin-Gheva, J. Dimitroulakos, Y. Wan
Writing, review, and/or revision of the manuscript: M.J. Atherton, J. Pol, S. Johnson-Obaseki, P.J. Villeneuve, J. Dimitroulakos, Y. Wan, B.D. Lichty
Administrative, technical, or material support (i.e., reporting or organizing data, constructing databases): K.B. Stephenson, J. Pol, C. Lefebvre, P.J. Villeneuve
Study supervision: J.-S. Diallo, B.D. Lichty
Other (developed Maraba MG1-based virus reagents): D.F. Stojdl

Acknowledgments

The authors thank Natasha Kazhdan, Tabassom Baghai, Jennifer E.L. Hanson, and Vanessa Garcia for technical assistance and Joe S. Mymryk for the gift of plasmids. This work was partially funded by Turnstone Biologics as well as grants from the Terry Fox Foundation and BioCanRx.

Grant Support

M.J. Atherton, F. Wang, C. Lefebvre, D.F. Stojdl, A. Nguyen, L. Chen, J.-S. Diallo, Y. Wan, and B.D. Lichty are partially funded by grants from the Terry Fox Foundation (TFF-122868) and BioCanRX (FY16/ES1). K.B. Stephenson, J.K. Nikota, D.F. Stojdl, and B.D. Lichty are partially funded and employed by Turnstone Biologics.

The costs of publication of this article were defrayed in part by the payment of page charges. This article must therefore be hereby marked *advertisement* in accordance with 18 U.S.C. Section 1734 solely to indicate this fact.

Received February 24, 2017; revised June 23, 2017; accepted September 1, 2017; published OnlineFirst September 14, 2017.

References

1. de Martel C, Ferlay J, Franceschi S, Vignat J, Bray F, Forman D, et al. Global burden of cancers attributable to infections in 2008: a review and synthetic analysis. Lancet Oncol 2012;13:607–15.
2. Lowy DR, Schiller JT. Reducing HPV-associated cancer globally. Cancer Prev Res 2012;5:18–23.
3. Torre LA, Bray F, Siegel RL, Ferlay J, Lortet-Tieulent J, Jemal A. Global cancer statistics, 2012. CA Cancer J Clin 2015;65:87–108.
4. Moore KA, Mehta V. The growing epidemic of HPV-positive oropharyngeal carcinoma: a clinical review for primary care providers. J Am Board Fam Med 2015;28:498–503.
5. Narisawa-Saito M, Kiyono T. Basic mechanisms of high-risk human papillomavirus-induced carcinogenesis: roles of E6 and E7 proteins. Cancer Sci 2007;98:1505–1511.
6. Beglin M, Melar-New M, Laimins L. Human papillomaviruses and the interferon response. J Interferon Cytokine Res 2009;29:629–35.
7. Bartkowiak T, Singh S, Yang G, Galvan G, Haria D, Ai M, et al. Unique potential of 4-1BB agonist antibody to promote durable regression of HPV+ tumors when combined with an E6/E7 peptide vaccine. Proc Natl Acad Sci USA 2015;112:E5290–5299.

8. van der Sluis TC, van der Burg SH, Arens R, Melief CJ. New approaches in vaccine-based immunotherapy for human papillomavirus-induced cancer. Curr Opin Immunol 2015;35:9–14.
9. van der Sluis TC, Sluijter M, van Duikeren S, West BL, Melief CJM, Arens R, et al. Therapeutic peptide vaccine-induced CD8 T cells strongly modulate intratumoral macrophages required for tumor regression. Cancer Immunol Res 2015;3:1042–51.
10. Skeate JG, Woodham AW, Einstein MH, Da Silva DM, Kast WM. Current therapeutic vaccination and immunotherapy strategies for HPV-related diseases. Hum Vaccines Immunother 2016;12:1418–29.
11. Lichty BD, Breitbach CJ, Stojdl DF, Bell JC. Going viral with cancer immunotherapy. Nat Rev Cancer 2014;14:559–67.
12. Mahoney DJ, Stojdl DF. Molecular pathways: multimodal cancer-killing mechanisms employed by oncolytic vesiculoviruses. Clin Cancer Res 2013;19:758–63.
13. Brun J, McManus D, Lefebvre C, Hu K, Falls T, Atkins H, et al. Identification of genetically modified Maraba virus as an oncolytic rhabdovirus. Mol Ther 2010;18:1440–9.
14. Pol JG, Zhang L, Bridle BW, Stephenson KB, Rességuier J, Hanson S, et al. Maraba virus as a potent oncolytic vaccine vector. Mol Ther 2014;22:420–9.
15. Le Boeuf F, Niknejad N, Wang J, Auer R, Weberpals JI, Bell JC, et al. Sensitivity of cervical carcinoma cells to vesicular stomatitis virus-induced oncolysis: Potential role of human papilloma virus infection. Int J Cancer 2012;131:E204–15.
16. Smyth GK. Linear models and empirical bayes methods for assessing differential expression in microarray experiments. Stat Appl Genet Mol Biol 2004;3:Article3.
17. Chung CH, Zhang Q, Kong CS, Harris J, Fertig EJ, Harari PM, et al. p16 protein expression and human papillomavirus status as prognostic biomarkers of nonoropharyngeal head and neck squamous cell carcinoma. J Clin Oncol 2014;32:3930–8.
18. Diallo J-S, Roy D, Abdelbary H, De Silva N, Bell JC. Ex vivo infection of live tissue with oncolytic viruses. J Vis Exp JoVE 2011. e2854, doi:10.3791/2854.
19. Thomas M, Pim D, Banks L. The role of the E6-p53 interaction in the molecular pathogenesis of HPV. Oncogene 1999;18:7690–700.
20. Münger K, Baldwin A, Edwards KM, Hayakawa H, Nguyen CL, Owens M, et al. Mechanisms of human papillomavirus-induced oncogenesis. J Virol 2004;78:11451–60.
21. Lai F, Kazdhan N, Lichty BD. Using G-deleted vesicular stomatitis virus to probe the innate anti-viral response. J Virol Methods 2008;153:276–9.
22. Rauschhuber C, Noske N, Ehrhardt A. New insights into stability of recombinant adenovirus vector genomes in mammalian cells. Eur J Cell Biol 2012;91:2–9.
23. Seder RA, Darrah PA, Roederer M. T-cell quality in memory and protection: implications for vaccine design. Nat Rev Immunol 2008;8:247–58.
24. Klebanoff CA, Gattinoni L, Restifo NP. CD8+ T-cell memory in tumor immunology and immunotherapy. Immunol Rev 2006;211:214–24.
25. Redeker A, Welten SPM, Baert MRM, Vloemans SA, Tiemessen MM, Staal FJT, et al. The quantity of autocrine IL-2 governs the expansion potential of CD8+ T cells. J Immunol 2015;195:4792–801.
26. Bridle BW, Nguyen A, Salem O, Zhang L, Koshy S, Clouthier D, et al. Privileged antigen presentation in splenic B cell follicles maximizes T cell responses in prime-boost vaccination. J Immunol 2016;196:4587–95.
27. Stevanović S, Draper LM, Langhan MM, Campbell TE, Kwong ML, Wunderlich JR, et al. Complete regression of metastatic cervical cancer after treatment with human papillomavirus-targeted tumor-infiltrating T cells. J Clin Oncol 2015;33:1543–50.
28. Klebanoff CA, Gattinoni L, Palmer DC, Muranski P, Ji Y, Hinrichs CS, et al. Determinants of successful CD8+T-cell adoptive immunotherapy for large established tumors in mice. Clin Cancer Res 2011;17:5343–52.
29. Eskander RN, Tewari KS. Immunotherapy: an evolving paradigm in the treatment of advanced cervical cancer. Clin Ther 2015;37:20–38.
30. Gunn GR, Zubair A, Peters C, Pan ZK, Wu TC, Paterson Y. Two Listeria monocytogenes vaccine vectors that express different molecular forms of human papilloma virus-16 (HPV-16) E7 induce qualitatively different T cell immunity that correlates with their ability to induce regression of established tumors immortalized by HPV-16. J Immunol 2001;167:6471–9.
31. Zwaveling S, Ferreira Mota SC, Nouta J, Johnson M, Lipford GB, Offringa R, et al. Established human papillomavirus type 16-expressing tumors are effectively eradicated following vaccination with long peptides. J Immunol 2002;169:350–8.
32. Moynihan KD, Opel CF, Szeto GL, Tzeng A, Zhu EF, Engreitz JM, et al. Eradication of large established tumors in mice by combination immunotherapy that engages innate and adaptive immune responses. Nat Med 2016;22:1402–10.
33. Garrido F, Aptsiauri N, Doorduijn EM, Garcia Lora AM, van Hall T. The urgent need to recover MHC class I in cancers for effective immunotherapy. Curr Opin Immunol 2016;39:44–51.
34. Malek TR, Castro I. Interleukin-2 receptor signaling: at the interface between tolerance and immunity. Immunity 2010;33:153–65.
35. Esensten JH, Helou YA, Chopra G, Weiss A, Bluestone JA. CD28 costimulation: from mechanism to therapy. Immunity 2016;44:973–88.
36. Apte RN, Dotan S, Elkabets M, White MR, Reich E, Carmi Y, et al. The involvement of IL-1 in tumorigenesis, tumor invasiveness, metastasis and tumor-host interactions. Cancer Metastasis Rev 2006;25:387–408.
37. van der Burg SH, Arens R, Ossendorp F, van Hall T, Melief CJM. Vaccines for established cancer: overcoming the challenges posed by immune evasion. Nat Rev Cancer 2016;16:219–33.
38. Melief CJM, van Hall T, Arens R, Ossendorp FBurg SH van der. Therapeutic cancer vaccines. J Clin Invest 2015;125:3401–12.
39. Campo MS. Animal models of papillomavirus pathogenesis. Virus Res 2002;89:249–61.